BRAND LOFTING ABOVE LARGE-SCALE FIRES

by

John P. Woycheese, Patrick J. Pagni
and Dorian Liepmann
Department of Mechanical Engineering
University of California
Berkeley, CA, 94720-1740, USA

Reprinted from the Second (2nd) International Conference on Fire Research and Engineering (ICFRE2), August 3-8, 1997, Gaithersburg, MD. Proceedings. Sponsored by the National Institute of Standards and Technology (NIST) and Society of Fire Protection Engineers (SFPE). Published by the Society of Fire Protection Engineers, Boston, MA, 1998.

Brand Lofting Above Large-Scale Fires

John P. Woycheese, Patrick J. Pagni, and Dorian Liepmann
Department of Mechanical Engineering
University of California
Berkeley, California

INTRODUCTION

Although lofting of burning brands in forest fires has received considerable attention [1-4], little research has quantified the transport of brands from burning structures. This mechanism of fire spread is of particular importance in post-earthquake and urban/wildland intermix fires [5]. The 20 October 1991 Oakland Hills Fire, which cost more than $1 billion, was propagated primarily by flaming brands deposited hundreds of meters ahead of the fire front [5]. Perry [6] estimated that for every burning house with a wood-shingle roof, 600 shingles were lofted. This model for brand lofting follows the seminal work of Taylor [7]. Previous studies by Tarifa et al. [8, 9] and Lee et al. [10, 11] made the assumption of a constant vertical velocity above the fire source. Here a burning house is more accurately represented as an axisymmetric pool fire with a Baum and McCaffrey plume [12].

ANALYSIS

Force Balance

Conservation of brand momentum [7] is

$$\frac{d}{dt}(mV) = \sum_i F_i \,, \tag{1}$$

where V is the particle velocity with respect to ground, F_i are forces on the particle, and m is the mass. A spherical body in a velocity field is affected by two forces: drag and gravity. The gravity force is

$$F_g = -mg \,, \tag{2}$$

where g is the acceleration due to gravity. The drag force is

$$F_d = \frac{1}{2} C_d \rho_a |W|^2 \frac{W}{|W|} A_c \quad , \tag{3}$$

where A_c is the cross-sectional area of the brand, ρ_a is the density of air, C_d is the drag coefficient, and W is the relative velocity of the plume to the particle, $W \equiv U - V$. The drag force acts in the direction of W with a strength proportional to the square of $|W|$. With the above, the force-balance, Eq. (1), becomes

$$\frac{d}{dt}(mV) = \frac{1}{2} \rho_a A_c C_d |W| W - mg \,. \tag{4}$$

The change in momentum in Eq. (4) offsets the drag and gravity forces. Schematics of the brand, coordinates, forces, and fire plume can be found in Figs. 1 and 2.

To pessimize the lofting problem, the fire plume velocity is assumed to be strictly vertical with the magnitude of the centerline of the plume. With time-dependent particle mass and velocity, the acceleration of the particle is

$$\frac{dV}{dt} = \frac{1}{2}\left(\frac{\rho_a A_c C_d}{m}\right)|W|W - \left(\frac{V}{m}\right)\frac{dm}{dt} - g. \quad (5$$

In this study, the brands are modeled as spheres to obtain an explicit dependence on size and to employ the available literature for C_d. The mass and cross-sectional area of a sphere, $m = (\pi d \rho_s)/6$ and $A_c = (\pi d^2)/4$, are introduced into Eq. (5), where ρ_s is the homogenized density of the particle and d its diameter. The acceleration becomes

$$\frac{dV}{dt} = \frac{3}{4}\left(\frac{\rho_a}{\rho_s}\right)\left(\frac{C_d}{d}\right)|W|W - V\left(\left(\frac{1}{\rho_s}\right)\frac{d\rho_s}{dt} + \left(\frac{3}{d}\right)\frac{dd}{dt}\right) - g \quad . \quad (6$$

The first term on the right-hand side of Eq. (6) is the acceleration of the particle due to drag. The second and third terms express the acceleration from the change in particle mass with respect to time ($d\rho_s/dt$ and dd/dt are < 0). The final term is the deceleration due to gravity.

Plume Model

Several models quantify the fire plume velocity field [7,12-14], each applicable to different conditions. This study uses a slightly modified version of the Baum and McCaffrey (B-M) plume model [12], which idealizes a fire as a low-momentum burner flame and separates the height above the burner into three distinct regions: continuous flame, intermittent flame, and plume (Regions I, II, and III in Fig. 2). In Region I, the flame is continuous and the combustion process heats the gasses within this region, increasing the gas velocity. Region II contains the full range of intermittent visible flame patches; the periodic action of these patches keeps the averaged centerline velocity constant in this region. Region III covers the non-combusting thermal plume above Region II, where the plume velocity decays due to entrainment of the surrounding air and turbulent spreading of the plume width.

The B-M centerline plume velocity is given by

$$U^*_{bm} = A_j (z^*)^{n_j}, \quad (7)$$

where $U^*_{bm} = U_{bm}/U_c$, $z^* = z/z_c$, $U_c = ((\dot{Q}_o g^2)/(\rho_a c_p T_o))^{1/5}$, $z_c = (\dot{Q}_o/((\rho_a c_p T_o)\sqrt{g}))^{2/5}$, and A_j and n_j are given in Table 1. $\dot{Q}_o$ is the rate of heat release for the fire and ρ_a, c_p, and T_o are the ambient density, specific heat, and temperature. A detailed derivation of the characteristic quantities is given in [15]. The centerline velocity is shown in dimensionless form in Fig. 3. To ensure that the equations are Lipshitz-continuous, the velocity between Regions I and II and between II and III is matched near $z^* = 1.32$ and 3.3 using two, fifth-order polynomials.

Table 1: Baum and McCaffrey Plume Velocity Parameters

Region (j)	Range	A_j	n_j
I	$0 \le z^* \le 1.32$	2.18	1/2
II	$1.32 \le z^* \le 3.3$	2.45	0
III	$z^* \ge 3.3$	3.64	-1/3

Diameter Regression Models

Two regression models are used in this study. Non-burning spheres clarify the particle dynamics, and a burning droplet in quiescent air provides more realistic lofting paths for combusting spherical brands. The brand mass loss is assumed to occur only by surface regression; i.e., a constant density is assumed. Density variation due to charring, forced flow, and comparison with experiments will be developed in future work. The regression rate for a non-burning sphere is

$$\frac{dd}{dt} = 0. \tag{8}$$

This trivial equation allows the determination of the maximum height to which a sphere of a given diameter can rise.

The burning-droplet problem models a spherical fuel particle combusting in an oxidizing, quiescent atmosphere. Although the combustion zone surrounding a spherical particle is not strictly spherical -- due to the buoyancy forces on the hot gases from combustion -- the burning-droplet equations assume spherical symmetry for simplicity [20,21]. The combustion is assumed to be quasi-steady; a surface mass balance relates the brand mass loss rate to the surface regression rate,

$$\dot{m} = -\frac{d}{dt}\left(\frac{\pi d^3 \rho_s}{6}\right) = -\frac{\pi d^2 \rho_s}{2}\left(\frac{dd}{dt}\right). \tag{9}$$

A surface energy balance provides a second expression for $\dot{m}$, due to heat feedback from the flame,

$$\dot{m} = 2\pi d \rho_a \mathcal{D} \ln(1 + B), \tag{10}$$

where $\mathcal{D}$ is the diffusivity of fuel vapor in air and B is the fuel mass transfer number. The Lewis number, $Le = \alpha/\mathcal{D}$, is assumed to be unity. See [20] for a discussion of this assumption. The two mass loss rates are equated to find the regression rate of the spherical brand diameter,

$$\frac{dd}{dt} = -4\alpha\left(\frac{\rho_a}{\rho_s}\right)\frac{\ln(1 + B)}{d}. \tag{11}$$

Initial Conditions

In this problem, there are three dependent variables, V, d, and z, and one independent variable, t. (U is determined by z from Eq. (7) and thus is not a separate dependent variable; ρ_s is assumed constant.) The velocity and acceleration of the brand are assumed to be zero at t=0 and

the density and diameter of the brand are known initially; only the initial height is not known *apriori*.

For the B-M plume model, there is a unique height, z_o, below which brands of a given initial diameter cannot be lofted. Brands can be lofted only where the relative velocity exceeds their terminal velocity; this holds for both combusting and non-combusting particles. Because the brand velocity is initially zero, W equals U_{bm}, which is always positive, and Eq. (6) reduces to

$$\frac{dV}{dt} = \frac{3}{4}\left(\frac{\rho_a}{\rho_s}\right)\left(\frac{C_d}{d}\right)|U_{bm}|^2 - g \tag{12}$$

at t = 0. The terms on the right side of Eq. (12) exactly balance when dV/dt = 0, which identifies the minimum height at which the plume can support a spherical particle of a given diameter. Substituting for Region I from Table 1 and solving for z_o, the initial brand height is

$$z_o = \left(\frac{z_c}{2.13^2}\right)\left(\frac{4}{3}\right)\left(\frac{d}{C_d}\right)\left(\frac{\rho_s}{\rho_a}\right)g. \tag{13}$$

Substituting for Region III from Table 1 and solving for z_{max}, the maximum loftable height is

$$z_{max} = \left(\frac{3}{4}\left(\frac{C_d}{d}\right)\left(\frac{\rho_a}{\rho_s}\right)\frac{3.64^2}{g}\right)^{1.5} z_c . \tag{14}$$

Drag Coefficient

The drag coefficient, C_d, primarily depends upon Reynolds Number and body shape. There are numerous equations in the literature correlating $C_d(Re)$ for spheres near terminal velocity [16-19]; that of Haider and Levenspiel [19] is accurate for $Re < 2.6 \times 10^5$. This equation,

$$C_d = \frac{24}{Re}(1 + 0.1806(Re)^{0.6459}) + \frac{0.4251(Re)}{Re + 6880.95}, \tag{15}$$

is shown in Fig. 4. The coupled set of Eqs. (13 or 14 and 15) must be solved iteratively because Cd($Re=(U_{bm}d)/\nu$).

Non-Dimensionalization

Maximum information, in terms of the minimum number of parameters, is extracted from equations that are dimensionless with respect to the appropriate characteristic quantities for each variable [21]. The equations to be non-dimensionalized are

$$\frac{dV}{dt} = \frac{3}{4}\left(\frac{\rho_a}{\rho_s}\right)\left(\frac{C_d}{d}\right)|U_{bm} - V|(U_{bm} - V) - V\left(\left(\frac{3}{d}\right)\frac{dd}{dt} + \left(\frac{1}{\rho_s}\right)\frac{d\rho_s}{dt}\right) - g, \tag{16}$$

dd/dt (either Eq. (8 or 11)), and dz/dt = V. Note that $d\rho_s/dt = 0$ is assumed here. The dimensionless variables and parameters are defined as

$$V^* = \frac{V}{U_c} \quad U^*_{bm} = \frac{U_{bm}}{U_c} \quad z^* = \frac{z}{z_c} \quad d^* = \frac{d}{d_c} \quad \rho^* = \frac{\rho_s}{\rho_c} \quad t^* = \frac{t}{t_c}, \tag{17}$$

where U_c and z_c are defined after Eq. (7) and $t_c = z_c/U_c = U_c/g$. C_d is a function of $Re = ((U_{bm} - V)d)/\nu$. Using Eqs. (17), the Reynolds number becomes

$$Re = (U^*_{bm} - V^*)d^*\left(\frac{d_c U_c}{\nu}\right), \tag{18}$$

where U_c is defined by the plume model. At this point, the Reynolds number will change with any variation in the characteristic velocity, i.e., different fire strength or ambient conditions. If $d_c \equiv \nu/U_c$, however, the Reynolds number becomes only a function of dimensionless variables. Therefore that choice for d_c is made and

$$Re = (U^*_{bm} - V^*_z)d^*. \tag{19}$$

Substituting Eqs. (17) into Eq. (16) gives

$$\frac{dV^*}{dt^*} = \frac{3}{4}\left(\frac{C_d}{\rho^* d^*}\right)\left(\frac{\rho_a}{\rho_c}\right)\left(\frac{t_c U_c^2}{\nu}\right)\left|U^*_{bm} - V^*\right|(U^*_{bm} - V^*) - V^*_z\left(\left(\frac{3}{d^*}\right)\frac{dd^*}{dt^*} + \left(\frac{1}{\rho^*}\right)\frac{d\rho^*}{dt^*}\right) - 1, \tag{20}$$

from which the characteristic density becomes

$$\rho_c = \frac{\rho_a t_c U_c^2}{\nu} = \left(\frac{\rho_a}{\nu}\right)\left(\frac{\dot{Q}_o \sqrt[3]{g}}{\rho_a c_p T_o}\right)^{3/5}. \tag{21}$$

The dimensionless brand acceleration equation is then

$$\frac{dV^*}{dt^*} = \frac{3}{4}\left(\frac{C_d}{\rho^* d^*}\right)\left|U^*_{bm} - V^*\right|(U^*_{bm} - V^*) - V^*\left(\left(\frac{3}{d^*}\right)\frac{dd^*}{dt^*} + \left(\frac{1}{\rho^*}\right)\frac{d\rho^*}{dt^*}\right) - 1. \tag{22}$$

The dimensionless brand diameter regression rate, from Eq. (8) or Eq. (11), is either

$$\frac{dd^*}{dt^*} = 0, \tag{23}$$

or

$$\frac{dd^*}{dt^*} = -\left(\frac{4\ln(1+B)}{d^*\rho^* Pr}\right), \tag{24}$$

where $Pr = \nu/\alpha$ is the Prandtl Number. $z^*(t^*)$, needed for U^*_{bm}, is obtained from

$$\frac{dz^*}{dt^*} = V^*. \tag{25}$$

Eqs. (22) and (25) must be solved simultaneously with one of Eqs. (23) or (24); the initial conditions are $t^* = 0$, $V^*_z(0) = 0$, $z^*(0) = z^*_o$, and $d^*(0) = d^*_o$.

The initial dimensionless particle height, from Eq. (13), is

$$z^*_o = 0.29\left(\frac{d^*_o \rho^*_o}{C_d}\right). \tag{26}$$

The maximum dimensionless loftable height, from Eq. (14), is

$$z^*_{max} = 31\left(\frac{C_d}{\rho^*_o d^*_o}\right)^{1.5}. \tag{27}$$

The initial Reynolds number can be calculated from

$$Re_o = d^*_o U^*_{bm}(z^*_o) = d^*_o U^*_{bm}\left(0.29\frac{d^*_o \rho^*_o}{C_d}\right), \tag{28}$$

because W reduces to U_{bm}, initially. For the burning-droplet case, Re_o is also the maximum Re

for that brand. When $1.2 \times 10^4 < Re < 2.6 \times 10^5$, the initial Reynolds number is

$$Re_o = 1.72(d_o^*)^{3/2}(\rho_o^*)^{1/2} \quad . \tag{29}$$

A plume with a particular ρ_o^* has a maximum loftable d_o^*. The terminal velocity of this $d_{o,max}^*$ is equal to the maximum plume velocity, which exists at $z_o^* = 1.28$ in Region I. Solving Eq. (26) with this z_o^*, a relationship can be developed between $d_{o,max}^*$ and ρ_o^*. Assuming that $C_d = 0.45$, a good approximation for $1.2 \times 10^4 < Re < 2.6 \times 10^5$, the maximum dimensionless loftable diameter is

$$d_{o,max}^* = 2\rho_o^{*-1} \tag{30}$$

for $\rho_o^* < 1/2700$.

LOFTING RESULTS

Non-Burning Spheres

Analyzing the path of non-burning spheres provides benchmarks against which other regression rates can be compared. In the non-combusting case, there are two dependent variables, V^* and z^*; one independent variable, t^*; and two constant parameters, ρ_o^* and d_o^*. Results are presented for $2000 \le d_o^* \le 15000$ and $\rho_{o,l}^* = 1/90000 \le \rho_o^* \le 1/7600 = \rho_{o,h}^*$ These dimensionless densities correspond to 50MW and 3GW pool fires for cedar wood ($\rho_s = 300$ kg/m^3) in air. The former approximates a house fire, while the latter approaches the intensity of the 20 October 1991 Oakland Hills Fire early in its development. The diameter range corresponds to brand sizes of 0.5 cm $\le d \le$ 3.5 cm for the 50MW fire and 0.2 cm $\le d \le$ 1.6 cm for the 3GW fire. The maximum loftable diameters for there two fires are 3.6 cm and 19 cm, respectively.

At $t^* = 0$, the particle is perturbed slightly upward, mimicking turbulence, to create a positive dV^*/dt^*, because $dV^*(z_o^*)/dt^* = 0$. This artificial boost is not needed for combusting brands, for which $dd^*/dt^* < 0$, and has a negligible effect on the paths of non-burning spheres. The particle accelerates upward rapidly through Region I, as shown in Fig. 5. The minimum lofting height increases with diameter for constant ρ_o^*; the larger particles have a higher terminal velocity that can be matched in the plume only at increased height. In Region II, acceleration decreases dramatically until the particle reaches its maximum velocity relative to ground slightly above $z^* = 3.3$. In Region III, the plume velocity (and thus the drag force) decreases with height until drag again balances gravity. $V^*(z_{max}^*) = 0$, but the plume is moving past the brand at the sphere's terminal velocity. The larger particles, with their higher terminal velocities, will come to rest at a lower height than the smaller particlesdue to the decay of $U_{bm}^*(z^*)$ in Region III.

In Fig. 6, the path for $d_o^* = 10000$ is plotted for $\rho_{o,l}^*$ and $\rho_{o,h}^*$. Although d_o^* is the same for both densities, the terminal velocity of a sphere decreases with decreasing density, so that the brand with $\rho_{o,l}^*$ is lofted to $z_{max}^* = 210$, as opposed to 6 for the higher density.

The initial and maximum lofting heights for non-combusting spherical particles are shown as functions of d_o^* parameterized in ρ_o^* in Fig. 7. The dotted lines demarcate the regions of the

plume model; particles are lofted in Region I ($z^* < 1.32$) and reach their maximum height in Region III ($z^* > 3.3$). For $1.2 \times 10^4 < Re < 2.6 \times 10^5$, $C_d = 0.45$ and the initial lofting height can be approximated by

$$z_o^* = 0.65 d_o^* \rho_o^*, \tag{31}$$

while the maximum loftable height is approximately

$$z_{max}^* = 9.5(\rho_o^* d_o^*)^{-1.5}. \tag{32}$$

A non-burning sphere travels a straight, vertical line accelerating from z_o^* and then decelerating to z_{max}^*. The paths of the combusting brands is more complex.

Spherical Firebrands

In this section, results are presented for combusting brands with burning-droplet regression rates. The same initial parameter ranges in d_o^* and ρ_o^* are used as for the non-burning spheres. The regression rate depends inversely on the the product $\rho_o^* d_o^*$, so that the diameter decreases faster the smaller the product is. The decrease in the brand diameter as it burns, parameterized in d_o^*, is shown in Fig. 8 for Pr = 0.706, B = 1.2, and $\rho_{o,h}^*$, which are typical for burning wood in air over a house fire. These parameters will be used throughout this section.

Unlike non-burning particles, the combusting brands need not be perturbed from z_o^*. The diameter regression causes an imbalance in the forces that loft the brands, as shown in Figs. 9 and 10. Drag is proportional to d^2 and gravity is proportional to d^3; therefore, as the diameter decreases, the drag force decreases more slowly that the gravity force. The brands start from z_o^* and rise until they burn out. Although smaller particles are lofted from lower heights, they accelerate more quickly and reach their burnout height, z_b^*, faster than the larger brands. The absolute velocity of the larger particles decreases to near zero in Region III and then accelerates slowly as they burn down to the small diameters. These larger brands spend a longer time at lower altitudes. Because of this, note in Fig. 9 that all of the brands with $d_o^* > 4000$ have the same z_b^*. The curves for height as a function of time, parameterized in ρ_o^*, are shown in Fig. 10. As ρ_o^* decreases, the burnout height increases. The shape of the curve for $\rho_{o,l}^*$ is similar to that for $d_o^* = 2000$ in Fig. 9, which indicates that $d_o^* = 10000$ is a small particle for $\rho_{o,l}^*$ as $d_o^* = 2000$ is a small particle for $\rho_{o,h}^*$.

The burnout height is shown as a function of d_o^* in Fig. 11. It is of note that all particles with $d_o^* > 4000$ burn out at the same height, $z_b^* = 56$, for $\rho_{o,h}^*$. This suggests that although the larger particles in the initial brand size distribution have longer lifetimes, the additional time is not available for them to attain a higher height because they move more slowly. The paths for a large range of particles collapse to a single curve for a particular density, as shown in Fig. 12 for $\rho_{o,h}^*$. The shape and values of that path are dependent on density, as illustrated by Fig. 13. z_b^* is greater than $z_{max}^*(d_o^*)$ because the decreasing diameter lowers the brand's terminal velocity. This increases the height at which the drag and gravity forces balance.

The particle velocity relative to the ground, as a function of height, is plotted in Fig. 14

(density dependence is illustrated in Fig. 15). The path of the brand with $d_o^* = 2000$ illustrates that not all of the brands for $\rho_{o,l}^*$ collapse to the same curve. Although this brand is subjected to the greatest acceleration of the four depicted in Fig. 14, it does not have sufficient size to approach the "collapse" curve.

For the burning-droplet model, the regression rate is ~ $1/d^*$ as shown in Eq. (24) so that the rate increases as the diameter tends to zero. As a result, the brand acceleration, Eq. (22), has a mass loss term that goes as $1/(d^*)^2$. As d^* approaches zero, the particle accelerates faster and faster. Thus, burning brands rapidly approach the local plume velocity as they burn out, as shown in Figs. 14 and 15. A three-dimensional view of $z^*(t^*)$, parameterized in d^*, is found in Fig. 16. Time increases from front-center to back-right; diameter increases from front-center to back-left; and height increases vertically. This figure combines all of the information in Figs. 8, 9, and 12 and also provides the initial particle height as a function of diameter, at $t^* = 0$, and the burnout height, for which $d^* = 0$, as function of burnout time. It shows that the larger ($d_o^* > 4000$ for $\rho_{o,h}^*$) particles simply take longer to get to a single burnout height, $z_b^* = 56$.

CONCLUSIONS

These calculations show that for a Baum-McCaffrey (B-M) plume there is a limit to the size of the loftable brand. For spheres, the maximum loftable initial diameter is given by

$$d_{o,max}^* \approx 2/\rho_o^* ,$$

where d^* and ρ^* are the dimensionless diameter and density. In dimensional terms,

$$d_{o,max} \approx 2\left(\frac{\rho_a}{\rho_s}\right)z_c = 2\left(\frac{\rho_a}{\rho_s}\right)\left(\frac{\dot{Q}_o}{(\rho_a c_p T_0)\sqrt{g}}\right)^{2/5} ,$$

where the symbols are defined in the notation. For cedar ($\rho_s = 300$ kg/m^3) spheres in a 50MW fire, $d_{o,max} = 3.6$ cm (1.5 in).

For the range, $1.2 \times 10^4 < Re < 2.6 \times 10^5$, that describes many spherical brands, $C_d \approx 0.45$ to within $\pm$ 5%. With this C_d, the minimum initial height from which a brand can be lofted by the B-M plume is

$$z_o^* \approx 0.65 d_o^* \rho_o^* .$$

In dimensional terms,

$$z_o \approx 0.65 d_o \left(\frac{\rho_s}{\rho_a}\right) .$$

For cedar spheres in a 50MW fire, the initial lofting height of a 3.6-cm-diameter sphere is 6 m (20 ft). Smaller spheres will have lower minimum lofting heights. The maximum height to which non-burning spheres could rise, i.e. the height at which their terminal velocity equals the plume velocity, has been calculated as a function of d^* and ρ^*. For $C_d \approx 0.45$, the maximum height is

$$z_{max}^* \approx 9.5(\rho_o^* d_o^*)^{-1.5} .$$

In dimensional terms,

$$z_{max} = 9.5\left(\frac{\rho_a}{\rho_s d_o}\right)^{1.5}\left(\frac{\dot{Q}_o}{(\rho_a c_p T_0)\sqrt{g}}\right).$$

For cedar in a 50MW fire, the maximum height is

$$z_{max}(d_o) = 0.1 d_o^{-1.5},$$

with d_o and z_{max} both in meters.

Additional calculations were made with the droplet burning model for the spherical brand regression rate. The results shown in Figs. 8 through 16 indicate that burning brands are consumed before they reach the maximum heights indicated above. A significant finding shown in these figures is that there is a collapse of the large end of the initial brand size distribution so that all brands greater than a certain diameter have the same burnout height ($z_b^* = 56$ for $d_o^* > 4000$ and $\rho_o^* = 1/7600$). For cedar spheres in a 50MW fire, $d_o^* = 4000$ corresponds to d = 0.9 cm (0.4 in) and z_b = 260 m (850 ft).

Future work will implement an improved burning model with a regression rate that includes forced-flow combustion. Propagation of brands downwind will be studied for simple ambient flow models. Eventually, these burning brands will be inserted as Lagrangian particles in the ALOFT Large Eddy Simulation model. This model was developed at NIST to describe the flow field above large fires and to incorporate terrain and ambient wind effects [22].

ACKNOWLEDGMENTS

We are grateful for the financial support provided by the Building and Fire Research Laboratory of the National Institute of Standards and Technology, U.S. D.O.C., Grant No. 60NANB3D1438, and by a student grant from the Educational and Scientific Foundation of the Society of Fire Protection Engineers.

REFERENCES

1. Muraszew, A., "Firebrand Phenomena," *Aerospace Report No. ATR - 74 (8165 - 01) - 1*, The Aerospace Corporation, El Segundo, 1974.
2. Muraszew, A., and Fedele, J.B., "Statistical Model for Spot Fire Hazard," *Aerospace Report No. ATR-77 (7588) - 1*, The Aerospace Corporation, El Segundo, 1976.
3. Albini, F.A., "Spot Fire Distance From Burning Trees: A Predictive Model," *General Technical Report No. INT-56*, USDA Forest Service Intermountain Forest and Range Experiment Station, Ogden, UT., 1979.
4. Albini, F.A., "Transport of Firebrands by Line Thermals," *Combustion Science and Technology*, **32**, pp. 277-288, 1983.
5. Pagni, P.J., "Causes of the 20 October 1991 Oakland Hills Conflagration," *Fire Safety Journal*, **21**:4, pp. 331-340, 1993.
6. Perry, W.C., *Wind and Fire II* (ME290F, Case Studies in Fire at the University of California at Berkeley), pp. 12, 1992.
7. Taylor, G.I., "Notes on Possible Equipment and Technique for Experiments on Icing on Aircraft", *Journal of Aerospace Sciences*, **25**, pp. 464, 1958.
8. Tarifa, C.S., del Notario, P.P., and Moreno, F.G., "On the Flight Paths and Lifetimes of Burning Particles of Wood," *Tenth Symposium (International) on Combustion*, pp. 1021-1037, The Combustion Institute, Pittsburg, 1965.
9. Tarifa, C.S., del Notario, P.P., Moreno, F.G., and Villa, A.R., "Transport and Combustion of Firebrands," *Final Report of Grants FG-SP-114 and FG-SP-146*, Vol. 2, USDA, Madrid, 1967.
10. Lee, S.-L., and Hellman, J.M., "Firebrand Trajectory Study Using an Empirical Velocity-Dependent Burning Law," *Combustion and Flame*, **15**:3, pp. 265-274, 1970.
11. Lee, S.-L., and Hellman, J.M., "Study of Firebrand Trajectories in a Turbulent Swirling Natural Convection

Plume," *Combustion and Flame*, **13**:6, pp. 645-655, 1989.
12. Baum, H.R. and McCaffrey, B.J., "Fire Induced Flow Field -- Theory and Experiment," *Fire Safety Science, Proceedings of the Second International Symposium*, ed. T. Wakamatsa et al., pp. 129-148, Hemisphere Washington, D.C., 1989.
13. Zukoski, E.E., "Fluid Dynamic Aspects of Room Fire," *Fire Safety Science, Proceedings of the First International Symposium*, ed. C.E. Grant and P.J.Pagni, pp. 1-30, Hemisphere, Washington, D.C., 1986.
14. McCaffrey, B.J., "Momentum Implications for Buoyant Diffusion Flames," *Combustion and Flame*, **52**, pp. 149-167, 1983.
15. Trelles, J. and Pagni, P.J., "Fire-Induced Winds in the 20 October 1991 Oakland Hills Fire", *Fire Safety Science, Proceedings of the 5th International Symposium*, IAFSS, Boston, 1997 in press.
16. Clift, R., Grace, J.R., and Weber, M.E., *Bubbles, Drops, and Particles*, Academic Press, New York, 1978.
17. Flemmer, R.L.C. and Banks, C.L., "On the Drag Coefficient of a Sphere," *Powder Technology*, **48**:3, pp. 217-221, 1986.
18. Turton, R. and Levenspiel, O., "A Short Note on the Drag Correlation for Spheres," *Powder Technology*, **47**, pp. 83-86, 1986.
19. Haider, A. and Levenspiel, O., "Drag Coefficient and Terminal Velocity of Spherical and Nonspherical Particles," *Powder Technology*, **58**, pp. 63-70, 1989.
20. Williams, F.A., "The Burning of a Fuel Particle in an Oxidizing Atmosphere," *Combustion Theory*, 2nd ed., pp. 52-69, Benjamin/Cummings Publishing, Menlo Park, 1985.
21. Pagni, P.J., "Diffusion Flame Analyses," *Fire Safety Journal*, **3**, pp. 273-285, 1980/81.
22. McGrattan, K.B., Baum, H.R., Walton, W.D., and Trelles, J., "Smoke Plume Trajectory from In Situ Burning of Crude Oil in Alaska -- Field Experiments and Modeling of Complex Terrain," NISTIR 5958, NIST, Gaithersburg, MD, Jan. 1997.

NOTATION

A	Baum and McCaffrey Plume Model Coefficient ( )
A_c	Cross-sectional area (m^2)
B	Mass transfer number ( )
c_p	specific heat of air (J/kg K)
C_d	Cefficient of drag ( )
d	diameter (m)
$\mathcal{D}$	Diffusivity of air (m^2/s)
F_i	Force (N)
g	Gravity (m / s^2)
Le	Lewis number ( )
m	particle mass (kg)
n	Exponent for Baum and McCaffrey Plume Model ( )
Pr	Prandtl Number ( )
$\dot{Q}_o$	Rate of heat release for the fire (W)
Re	Reynolds Number ( )
T_o	Ambient temperature (K)
U	Vector-valued velocity of surroundings (m/s)
U_{bm}	Scalar Baum and McCaffrey centerline plume velocity (m/s)
V	Scalar particle velocity relative to ground (m/s
W	Scalar relative velocity of a particle to its surroundings (m/s)
z	Vertical height of particle (m)
z_b	Burn-out height of particle (m)
z_o	Initial height of particle in lofting phase (m)
α	Thermal diffusivity of air (m^2/s)
ν	Kinematic viscosity of air (m^2/s)
ρ	density (kg/m^3)

Superscript

*	Dimensionless variable

Subscripts

a	Air
c	Characteristic Constant
j	Region of Baum and McCaffrey or Modified Baum and McCaffrey plume model
l	Height limit
s	Sphere

1. Empty brackets denote dimensionless quantities.

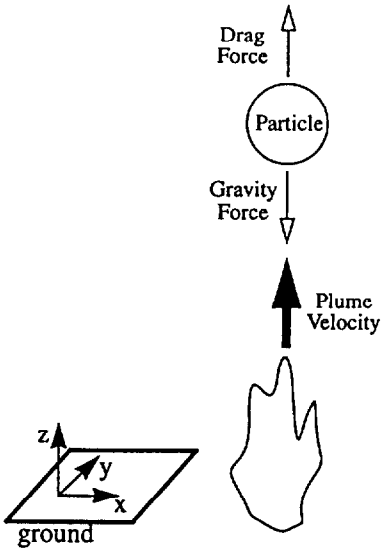

Figure 1: Force balance on a brand in a velocity field along the plume centerline, where horizontal velocities are assumed to be zero.

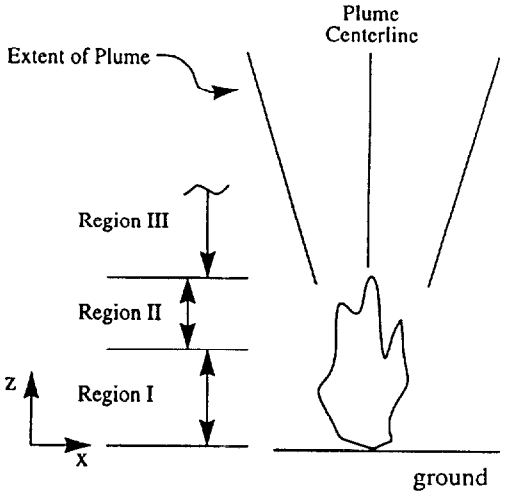

Figure 2: Visual representation of the plume model developed by Baum and McCaffrey [12], including the three regions described in the text.

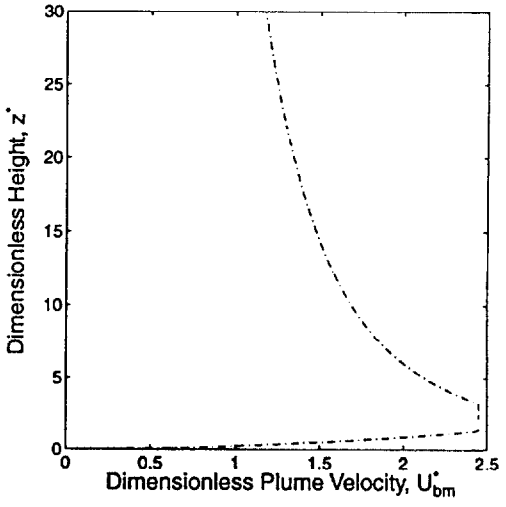

Figure 3: Profile of the centerline velocity above a fire using the plume model developed by Baum and McCaffrey [12].

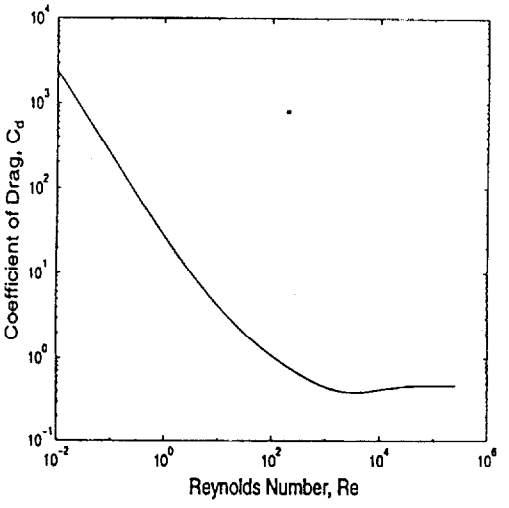

Figure 4: Graph of the empirical fit by Haider and Levenspiel [19] for the coefficient of drag as a function of Reynolds Number, valid for $Re < 2.6 \times 10^5$

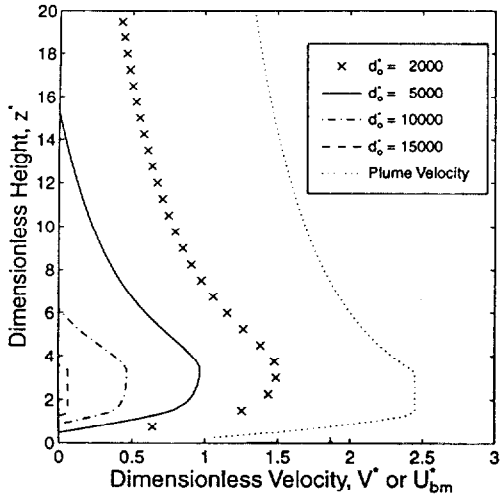

Figure 5: Plot of the velocity relative to ground for non-burning particles. The plume velocity has been included for reference. This figure gives the results for three particles with diameters $d_o^* = 2000$, 5000, 10000, and 15000 for $\rho_o^* = 1/7600$.

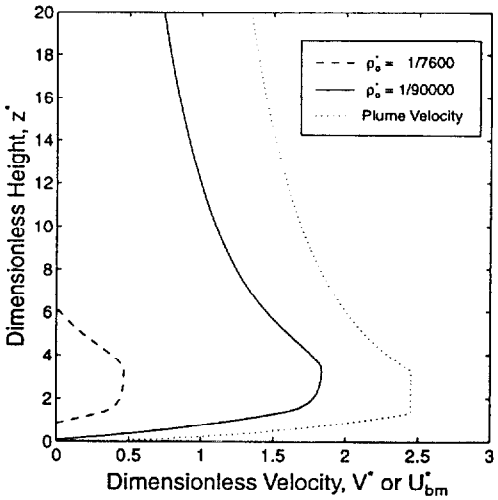

Figure 6: Plot of the velocity relative to ground for non-burning particles. The plume velocity has been included for reference. This figure gives the results for two densities, $\rho_o^* = 1/7600$ and 1/90000, and an initial diameter of $d_o^* = 10000$.

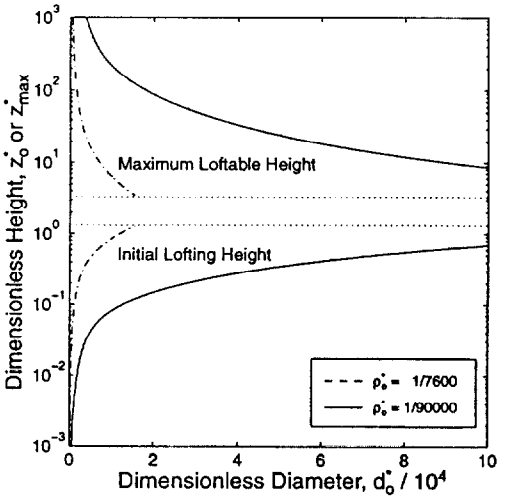

Figure 7: Minimum height at which the drag force exceeds that due to gravity as a function of diameter and density. Pr = 0.706.

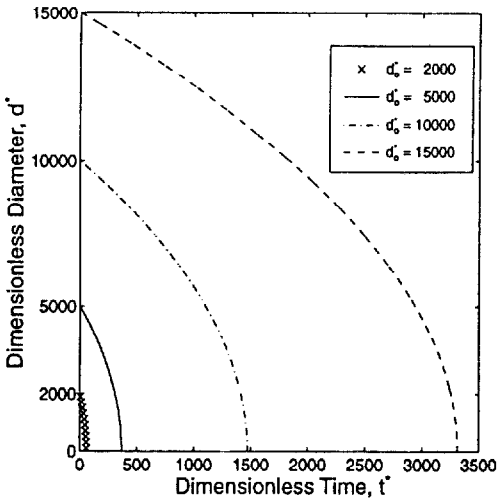

Figure 8: Diameter as a function of time for a the indicated initial diameters for density of $\rho_o^* = 1/7600$, Pr =0.706, B = 1.2, and a burning-droplet regression rate.

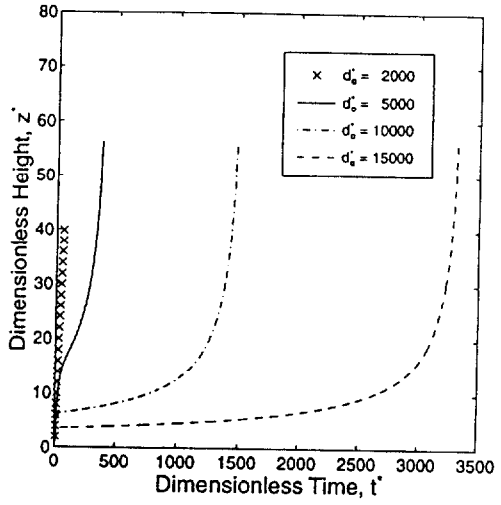

Figure 9: Plots of particle height as a function of time for the indicated initial diameters and a density of $\rho_o^* = 1/7600$, Pr = 0.706, B = 1.2, and a burning-droplet diameter regression.

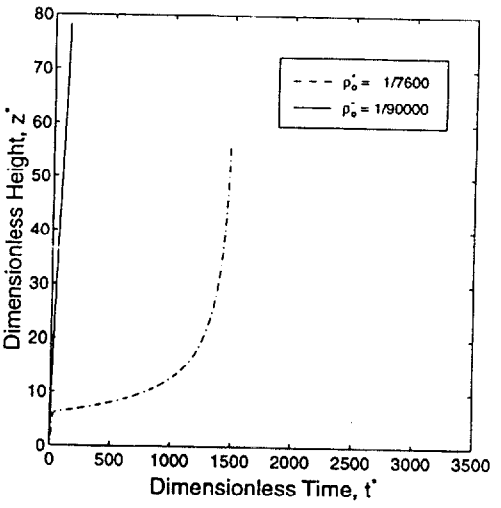

Figure 10: Plots of particle height as a function of time for the indicated densities and an initial diameter of $d_o^* = 10000$, Pr = 0.706, B = 1.2, for a burning-droplet diameter regression.

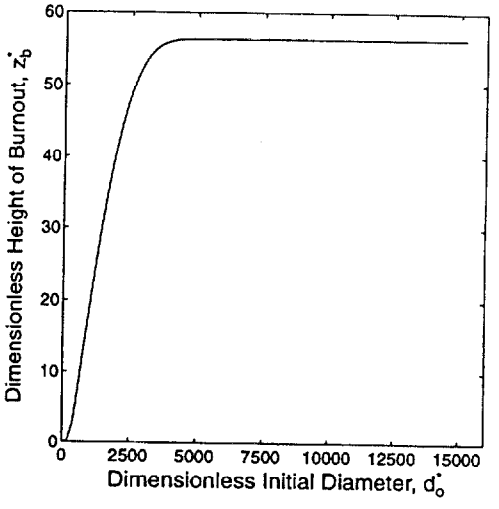

Figure 11: Maximum height to which particles of a given initial diameter can rise before burning out for $\rho_o^* = 1/7600$, Pr = 0.706, B = 1.2, and a burning-droplet regression rate.

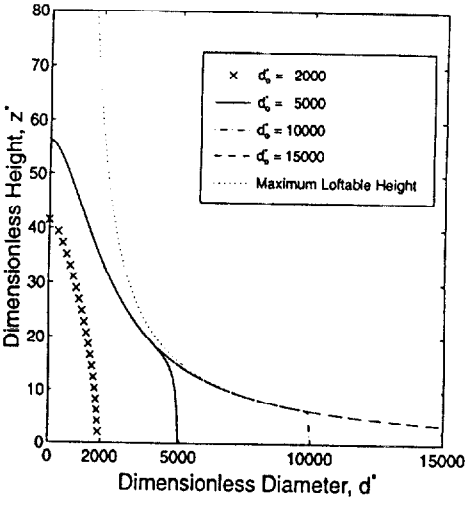

Figure 12: Particle height as a function of diameter for the initial diameters indicated and for a density of $\rho_o^* = 1/7600$, Pr = 0.706, and B = 1.2 for burning-droplet diameter regression. The "Maximum Loftable Height" is the height to which a non-burning particle of a particular diameter would rise.

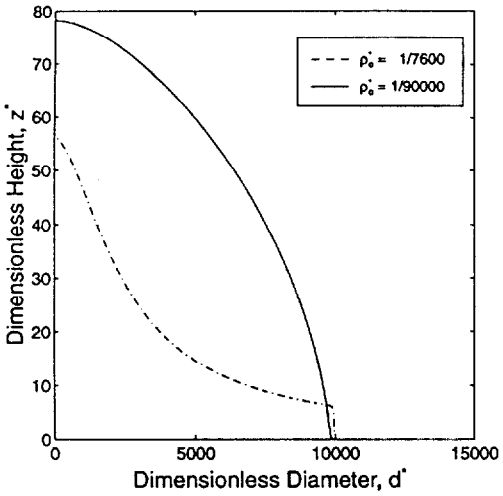

Figure 13: Particle height as a function of diameter for the densities indicated and for an initial diameter of $d_0^* = 10000$ for a burning-droplet regression rate. Pr = 0.706 and B = 1.2.

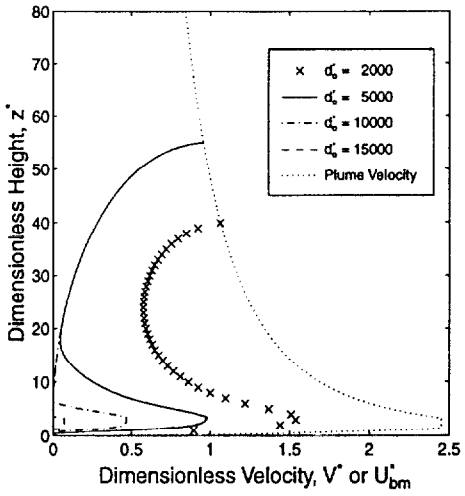

Figure 14: Particle height as a function of particle velocity relative to ground for a density of $\rho_0^* = 1/7600$ for a burning-droplet regression rate. The plume velocity has been included for reference. Pr = 0.706 and B = 1.2.

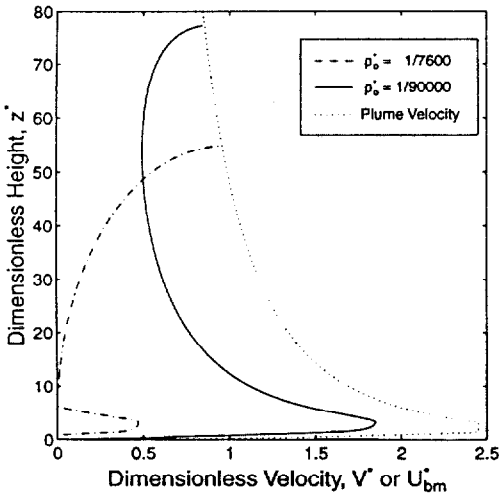

Figure 15: Particle height as a function of particle velocity relative to ground for a diameter of $d_0^* = 10000$ and a burning-droplet regression rate. The plume velocity has been included for reference. Pr = 0.706 and B = 1.2.

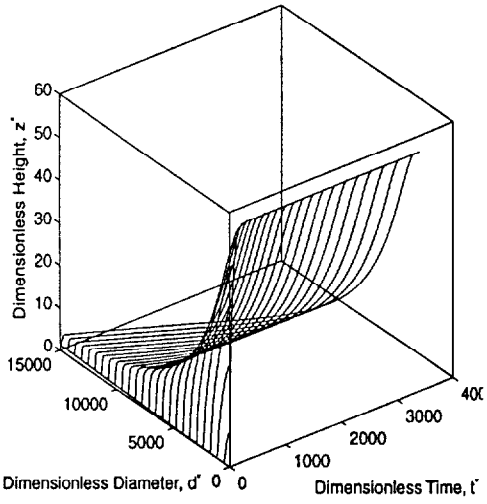

Figure 16: Three-dimensional representation of $z^*(t^*)$ parameterized in d^* for a sphere with a burning droplet regression rate. Curves are depicted in d_0^* in increments of 600 with $\rho^* = 1/7600$, Pr = 0.706, and B=1.2.